International Journal for Multiscale Computational Engineering, 19(5):1–15 (2021)

A CDM-BASED BINARY MODEL FOR THE PROGRESSIVE DAMAGE PREDICTION OF SiC/SiC CERAMIC MATRIX COMPOSITES UNDER TENSION LOADING

Jaedal Jung & Sergio L. dos Santos e Lucato*

Teledyne Scientific & Imaging, 1049 Camino Dos Rios, Thousand Oaks, California 91360, USA

*Address all correspondence to: Jaedal Jung, Teledyne Scientific & Imaging, 1049 Camino Dos Rios, Thousand Oaks, California 91360, USA; Tel.:+1 805 373 4249; Fax: +1 805 373 4017, E-mail: jaedal.jung@teledyne.com

Original Manuscript Submitted: 8/15/2021; Final Draft Received: 11/8/2021

In this paper, two benchmarking exercises for advanced ceramic matrix composites (CMCs)-challenge problem #1 and #2 of the Enhanced Physics-Based Prognosis and Inspection of CMC (EPPIC) program have been conducted to assess the capability of the continuum damage mechanics (CDM)–based binary model (BM) for progressive damage prediction in two SiC/SiC CMC systems: GEA SiC/SiC and S200H. The damage evolution laws of the equivalent matrix and fiber tows in the BM are first calibrated using provided/existing experimental data, and the calibrated model is then used to predict the damage onset and propagation in tension test specimens of GEA SiC/SiC and S200H. The overall strengths and weaknesses of the current modeling approach are discussed through rigorous comparison between the blind model predictions and the experimental validation data.

KEY WORDS: *CDM-based binary model, SiC/SiC ceramic matrix composites, benchmarking exercises*

1. INTRODUCTION

Ceramic matrix composites (CMCs) are an attractive material for structural component applications in gas turbine engines primarily due to their low weight and high mechanical performances at elevated temperatures. A growing number of manufacturers are adopting CMC technology to improve the performance of gas turbine engine components (Zivic et al., 2021). Along with the advent of the new technology, various finite element method (FEM)–based numerical approaches to predict damage growth and tolerance in CMCs also have been developed to support its development (Müzel et al., 2021). Progressive damage models are well-developed for metal-based components, but they are still in their infancy for CMCs. For this reason, the United States Air Force Research Laboratory (AFRL) has been interested in understanding and assessing state-of-the-art damage analysis models for CMCs. Against such a background, AFRL launched and recently completed the Enhanced Physics-Based Prognosis and Inspection of CMC (EPPIC) program (Jefferson et al., 2021)—a benchmarking program to pursue the above objective. As one of the modeling team members, Teledyne Scientific Company (TSC) participated in this program to benchmark the capability of the TSC damage model for progressive damage prediction in CMCs through a series of calibration and validation tests, including blind predictions.

The TSC progressive damage model, implemented in a finite element method framework, was devised based on the binary model (BM) for textile composites (Cox et al., 1994; Xu et al., 1995; McGlockton et al., 2003). In the binary model, each tow of a weave architecture is modeled as a string of 1D elements representative of the tow's axial stiffness. The equivalent matrix, the so-called effective medium, surrounding the tows is modeled as 3D elements representative of matrix-dominated composite properties, including transverse stiffness, shear stiffness, and Poisson's ratio. To accurately predict the onset and propagation of damage in CMCs, the TSC damage model allows for two

modeling approaches that can be used separately or combined in the BM framework: (i) a continuum damage model based on continuum damage mechanics (CDM) and (ii) a discrete crack model based on fracture mechanics. The continuum damage model is appropriate for describing distributed microcracking damage, while the discrete crack model is suitable for modeling one or more dominant cracks (Fang et al., 2017). In this paper, the CDM-based BM combined with an element deletion method is employed to conduct benchmark exercises.

In the benchmark study, two different SiC/SiC (silicon carbide fibers and silicon carbide matrices) CMC systems are investigated: the first CMC system consists of Prepreg Tape Silicon Melt Infiltrated Hi-Nicalon™-S/BN/Si_3N_4/SiC in a unidirectional fiber architecture with a $[0/30/60/90]_s$ layup, called GEA SiC/SiC from GE Aviation; and the second consists of Hi-Nicalon™ fibers with a BN/Si_3N_4 coating in an 8HSW (eight-harness satin weave) architecture with a $[0/90]_{2s}$ layup, called S200H from COI Ceramics, Inc. The model is first calibrated using a set of calibration data to successfully assess the ability of the CDM-based BM to predict damage evolution in the SiC/SiC CMCs. Once the model calibration has been completed, a series of blind predictions is performed for challenge problems. These predictions are then compared to experimental measurements, i.e., validation data [for more details about the validation tests, we shall refer the reader to Pierce et al. (2021)]. Based on the prediction results of the validation tests for the challenge problems, the overall strengths and weaknesses of the CDM-based BM approach are discussed in this paper.

The benchmark exercises to predict the creep and fatigue behavior of these two materials were also performed using newly developed BM-based modeling approaches with more of an empirical nature. However, we will not discuss the capability of these modeling approaches here; that will be addressed in a future publication.

The remainder of this paper is organized as follows: the challenge problems for GEA SiC/SiC with a unique layup and S200H with two staggered holes are stated in Section 2; the CDM-based BM approach and the model calibration procedure for tension tests are briefly described in Section 3; Section 4 provides the model parameters and material properties; Section 5 provides computational environments used in finite element analysis (FEA); the calibrated models are presented in Section 6; the blind predictions for the challenge problems are shown and compared to validation data in Section 7; and finally, Section 8 provides a summary, concluding remarks, and potential future work.

2. DESCRIPTION OF CHALLENGE PROBLEMS

2.1 Challenge Problem #1: Tensile Behavior of GEA SiC/SiC with a Unique Layup

The first benchmark exercise is to perform blind predictions of stress-versus-strain behavior for a tension test specimen of GEA SiC/SiC with the unique layup at 23°C, 816°C, and 1316°C. The blind predictions for tensile stress-versus-strain behavior and the tensile properties of modulus, proportional limit, ultimate tensile strength, and strain to failure will be compared to experimental validation data. The specific configurations and features of the tensile test specimen are as follows:

- Length = 150 mm; width = 12 mm; gauge length = 28 mm; gauge width = 8 mm; radius = 317 mm; thickness = 1.6 mm
- Layup: $[0/30/60/90]_s$
- Unidirectional weave
- Fiber volume fraction: 25%–28%

2.2 Challenge Problem #2: Tensile Behavior of S200H with Unique Features

The second benchmark exercise is to perform blind predictions of net section stress versus extensometer displacement behavior for a tension test specimen of S200H with a unique feature (two staggered holes) at 23°C, 982°C, and 1200°C. The blind predictions for tensile net section stress versus extensometer displacement traces and the tensile properties (using net section stress) of modulus, proportional limit, ultimate tensile strength, and axial extensometer

displacement to failure will be compared to experimental validation data. Here, the net section is defined as going through one of the holes. The specific configurations and features of the tensile test specimen are as follows:

- Length = 150 mm; width = 14 mm; gauge length = 28 mm; gauge width = 10 mm; radius = 317 mm; thickness = 2.3 mm
- Two holes: 2 mm in diameter; spaced 3 mm apart; centered 3.5 mm from the edge of the specimen
- Layup: $[0/90]_{2s}$
- Eight-harness satin weave (8HSW)
- Ends per inch (EPI): 22 × 22

3. MODELING APPROACH AND CALIBRATION

In this study, the binary model (BM) was used to simulate the nonlinear mechanical behavior of targeted composite materials. The BM was first devised by Cox et al. (1994) to analyze diverse forms of textile composites such as 3D weaves and braids, integral structures, stitched components, and knitted fabrics. It then turned out that this modeling approach was computationally efficient for large structural components and highly adaptable to a finite element (FE) model. In general, as illustrated in Fig. 1, the BM consists of two components: (i) an equivalent matrix (a.k.a. an effective medium) and (ii) fiber tows embedded within the equivalent matrix, each of which is constructed by 3D solid (continuum) elements and 1D line elements in an FE model, respectively. The equivalent matrix represents matrix-dominated composite properties such as longitudinal/transverse stiffness and Poisson's ratio, while the fiber tows represent 2D/3D weave architectures. The above two independent components interact with each other in a single system (i.e., the BM framework) to effectively account for the mechanical behavior of textile structural composites. For instance, in an FE model, the nodal degrees of freedom (e.g., displacement and temperature) of the fiber tow element (embedded element) are constrained to the interpolated values of the corresponding nodal degrees of freedom of the equivalent matrix element (host element).

Since the BM was initially developed on the basis of continuum damage mechanics (CDM) (Murakami, 2012), the mechanical behavior of the equivalent matrix and fiber tows of the BM is governed by a continuum damage constitutive law, as given below:

$$\sigma = (1 - d)E^0\varepsilon \tag{1}$$

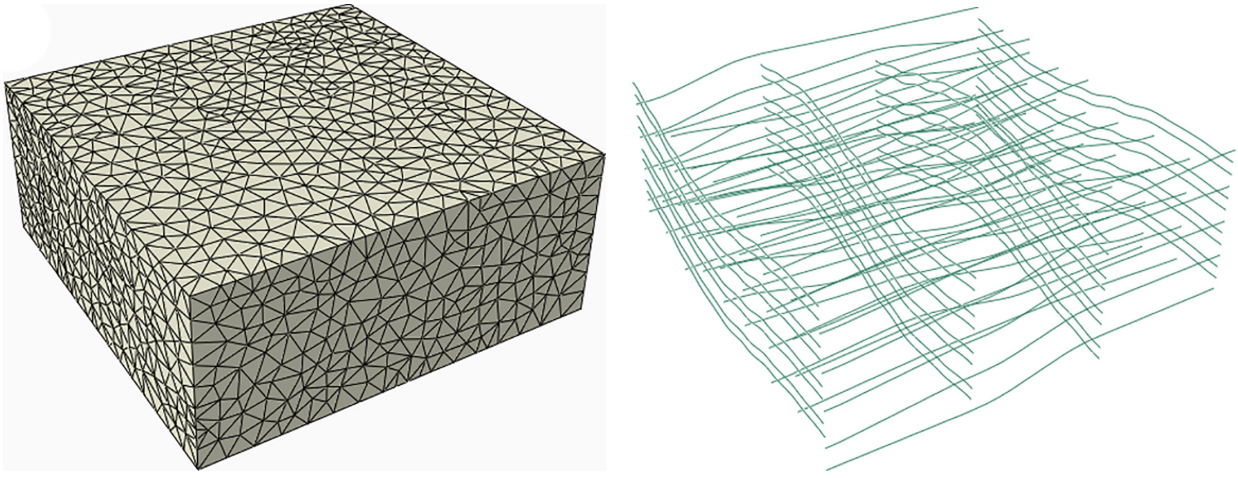

(a) (b)

FIG. 1: (a) Equivalent matrix (3D solid element) and (b) fiber tows (1D line element) in binary model for an FE analysis

where ε denotes the elastic strain; E^0 denotes the elastic modulus of the undamaged material; and d, a damage variable ($0 \leq d \leq 1$), is defined as a function of the residual stiffness E of the damaged material:

$$d = 1 - (E/E^0) \tag{2}$$

In accordance with the CDM theory, the material stiffness in the BM is gradually degraded with increasing displacement/strain due to the progressive loss of material integrity induced by microcrack initiation and growth. Thus, the damage evolution laws of the BM with respect to the equivalent matrix and fiber tows can be defined in terms of the elastic modulus and the strain. In particular, the damage behavior for the elastic modulus of the equivalent matrix and fiber tows (E_m and E_f) can be estimated through the model calibration process where iterative FE simulations are carried out until the best fit between the experimental and simulated stress–strain response is found. In the calibration, the initial E_m is calculated using the initial tangent stiffness of the composite stress–strain curve and the fiber volume fraction V_f. Based on the tensile damage process in CMCs, as illustrated in Fig. 2, beyond the elastic regime, the E_m is first degraded to match the modulus of the composite. When the E_m reaches a certain lower threshold (varied on a case-by-case basis), we assume that E_f starts to degrade. Then, the calibration for E_f is pursued until failure occurs. The model calibration must be conducted in advance to determine the damage evolution laws of E_m and E_f of the standard composite material. The calibrated E_m and E_f will be used for the blind predictions of the targeted composite.

Additionally, the fiber tow failure conditions are defined in the model calibration to capture tow rupture events. To this end, the current BM used in this benchmarking study adopts an element deletion method. Fiber tow elements satisfying the failure conditions are removed during virtual simulations. Since the element deletion method has a strong dependence of the crack path on the background mesh size and refinement due to localized quantities (e.g., displacement, strain, and stress), a small enough mesh is required to improve solution accuracy and computational convergence (Crété et al., 2014). The reasonable size of the mesh for simulations can be estimated through mesh sensitivity analysis. However, the global damage progression direction is the same regardless of the mesh size when using this modeling approach. This mesh sensitivity issue with finite element solutions can be mitigated by using a nonlocal damage approach (Geo et al., 2018).

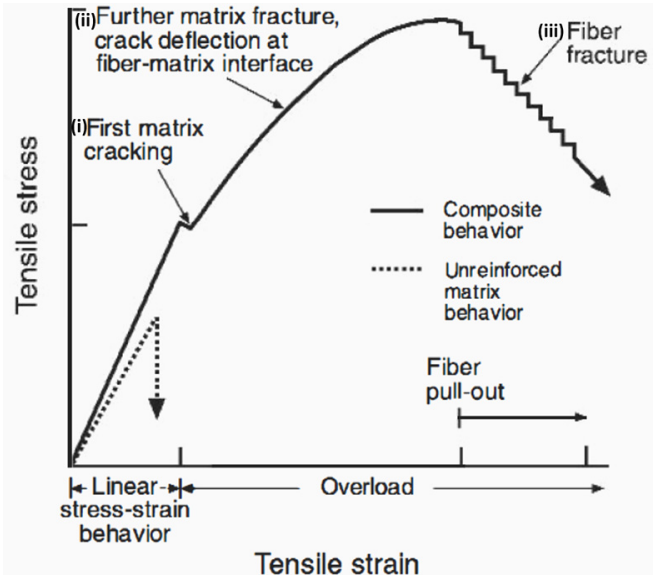

FIG. 2: Three major elements of the damage process in continuous fiber-reinforced CMCs under axial tension: (i) matrix cracking, (ii) fiber-matrix interfacial failure, and (iii) fiber fracture (reprinted from DiCarlo and Dutta with permission from the Purdue Research Foundation, Copyright 1995)

4. MODEL PARAMETERS AND MATERIAL PROPERTIES

According to Section 3, the damage variable d for the equivalent matrix and the fiber tows can be defined, respectively, as

$$d_m = 1 - (E_m/E_m^0); \quad d_f = 1 - (E_f/E_f^0) \tag{3}$$

Here, depending upon the value of the local strain (ε_m and ε_f), the piecewise linear damage evolution function for the elastic modulus (E_m and E_f) is determined through the model calibration process, i.e.,

$$E_m = f(\varepsilon_m); \quad E_f = f(\varepsilon_f) \tag{4}$$

The mechanical behavior of the equivalent matrix and fiber tows is governed by the following damage constitutive laws:

$$\sigma_m = (1 - d_m)E_m^0\varepsilon_m; \quad \sigma_f = (1 - d_f)E_f^0\varepsilon_f \tag{5}$$

The material properties for the equivalent matrix and fiber tows of two SiC/SiC CMCs, GEA SiC/SiC, and S200H, are presented in Tables 1 and 2, respectively. The elastic modulus of the equivalent matrix and fiber tows (E_m and E_f) are not specified in the tables because each modulus will be determined by the model calibration at different temperatures. The coefficient of thermal expansion (CTE) of each SiC/SiC composite shown in Fig. 3 is considered as that of its corresponding matrix and fiber tows in this benchmarking study.

5. COMPUTATIONAL ENVIRONMENTS

For the FE analysis of the calibration and blind prediction, the equivalent matrix and fiber tows were constructed by using approximately 39,000 linear brick elements and 23,000 truss elements, respectively. Computational simulations were carried out with version 6.17 of commercial software Abaqus via a user material subroutine (UMAT) on a workstation with Dual Intel Xeon Gold @ 3.4 GHz processors, 64 GB physical memory, and 12 CPU cores. The total computational time (wall-clock time) required to complete a single simulation in parallel on 10 CPU cores was about 420 s. About 20 simulations were required in each model calibration to determine the damage evolution laws and the tow rupture conditions.

TABLE 1: Material properties for equivalent matrix

Properties	GEA SiC/SiC	S200H
Young's modulus, E_m (GPa)	To be calibrated	To be calibrated
Poisson ratio, ν	0.18	0.12
Coefficient thermal expansion, α_m ($°C^{-1}$) α_m	See Fig. 3(a)	See Fig. 3(b)

TABLE 2: Material properties for fiber tows

Properties	GEA SiC/SiC	S200H
Young's modulus, E_f (GPa)	To be calibrated	To be calibrated
Tow area,† A_f (mm^2)	0.057	0.077
Coefficient thermal expansion, α_f ($°C^{-1}$)	See Fig. 3(a)	See Fig. 3(b)

†According to the *Composite Materials Handbook*, No. MIL-HDBK-17 (Department of Defense, 2002), a single tow generally consists of hundreds/thousands of filaments bundled together, and the cross-sectional area of the tow contains only the cumulative sum of the cross-sectional areas of all individual filaments within the bundle. The space between filaments is not counted in its cross-sectional area. Therefore, the tow cross-sectional areas of GEA SiC/SiC and S200H in this study were estimated using Hi-Nicalon™ Type-S and Hi-Nicalon™ ceramic fiber tow properties, respectively (e.g., the total number of filaments per tow and filament diameter), provided by COI Ceramics, Inc.

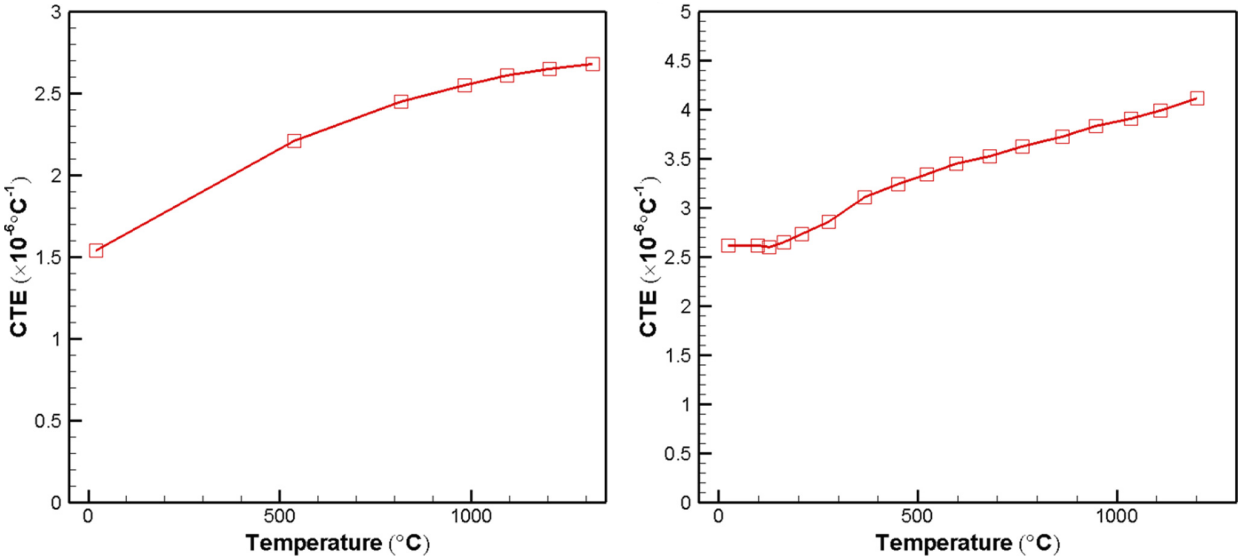

(a) (b)

FIG. 3: CTE (coefficient of thermal expansion) of the (a) GEA SiC/SiC and (b) S200H as a function of temperature (Jefferson et al., 2021)

6. CALIBRATION OF MODEL

6.1 Model Calibration for Challenge Problem #1

The stress–strain experimental data for the panel with a layup of $[0/90]_{2s}$ (provided from GE Aviation) was chosen for the model calibration for GEA SiC/SiC material. Based on the given geometric information for the tensile specimen of GEA SiC/SiC, the 3D virtual specimen for the model calibration is generated with the Teledyne composite framework (see Appendix A).

- Length = 6 in; width = 0.5 in; gauge length = 1.1 in; gauge width = 0.4 in; radius = 14.5 in; thickness = 0.063 in
- Layup: $[0/90]_{2s}$
- Unidirectional weave
- Fiber volume fraction: 25%–28%

The GEA SiC/SiC tension specimen, virtually constructed for the model calibration, is displayed in Fig. 4. E_m and E_f of the GEA SiC/SiC material are determined through the model calibration, as explained in Section 3. The resulting E_m and E_f are plotted as a function of strain in Figs. 5(a) and 5(b), respectively. Using the BM with the calibrated damage evolution laws for the equivalent matrix and fiber tows, the stress–strain responses[†] for the composite are simulated and plotted with a set of calibration data in Fig. 6, which shows that the simulation results agree well with the calibration data. The failure conditions of the fiber tows, determined in the model calibration at each temperature of 23°C, 816°C, and 1316°C, are presented in Table 3.

[†]For the composite stress–strain curve in this study, unless otherwise mentioned, the stress was calculated by using (i) the simulated force applied to the composite specimen and (ii) the cross-sectional area (gauge width × thickness), and the strain was measured with the virtual strain gauge attached to the surface of the specimen.

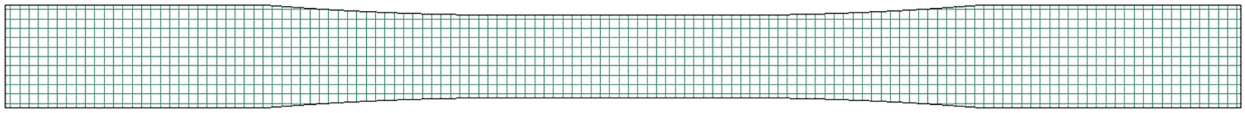

FIG. 4: The 3D virtual GEA SiC/SiC specimen with $[0/90]_{2s}$ and a unidirectional weave used in BM calibration

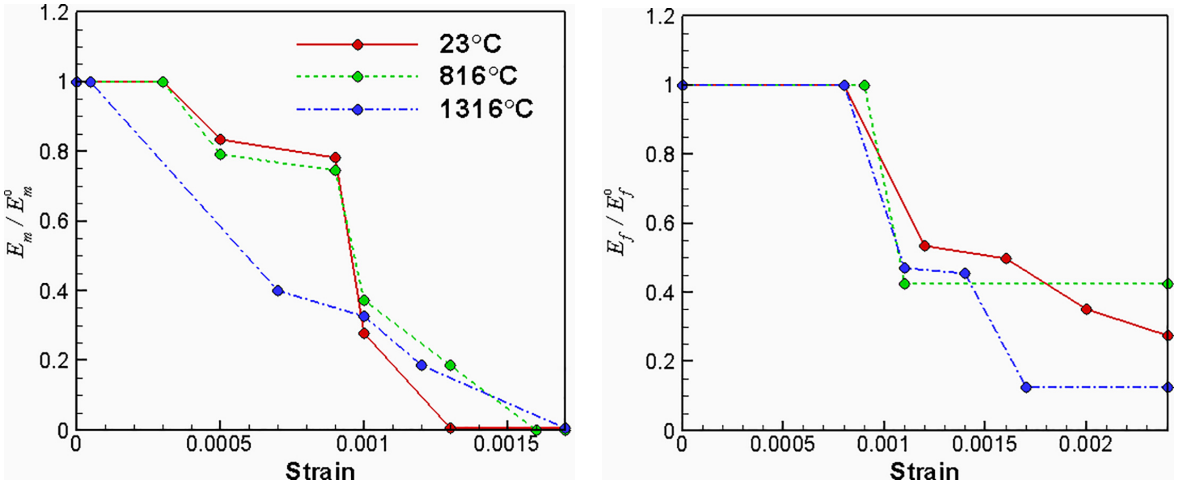

(a) (b)

FIG. 5: Calibrated damage evolution laws for (a) the equivalent matrix E_m and (b) the fiber tows E_f. Here, the superscript "0" of E_m and E_f denotes the undamaged elastic modulus.

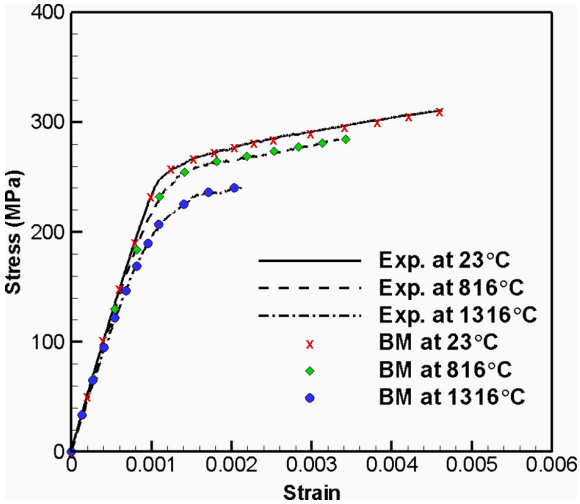

FIG. 6: Experimental measurements (black lines) versus BM predictions (symbols) for the tensile test of GEA SiC/SiC

6.2 Model Calibration for Challenge Problem #2

Similarly, the stress–strain experimental data for the panel with a layup $[0/90]_{2s}$ was chosen for the model calibration for S200H material. The 3D virtual specimen for the model calibration is prepared by using the Teledyne composite framework (see Appendix A). The geometric configurations and features of the tensile specimen of S200H are listed below:

TABLE 3: Fiber tow rupture conditions, determined in model calibration for GEA SiC/SiC

Temperature (°C)	Fiber tow strain (mm/mm)
23	4.35×10^{-3}
816	3.25×10^{-3}
1316	2.0×10^{-3}

- Length = 178.04 mm; width = 15 mm; gauge length = 28 mm; gauge width = 8 mm; radius = 50 mm; thickness = 2.24 mm
- Layup: $[0/90]_{2s}$
- Eight-harness satin weave (8HSW)
- Ends per inch (EPI): 22 × 22

The virtually generated S200H tension specimen for the model calibration is illustrated in Fig. 7. The calibration outcomes for the damage behavior of E_m and E_f and the failure conditions are presented in Fig. 8 and Table 4, respectively. The resulting stress–strain responses of the composite are in good agreement with experimental calibration data, as shown in Fig. 9.

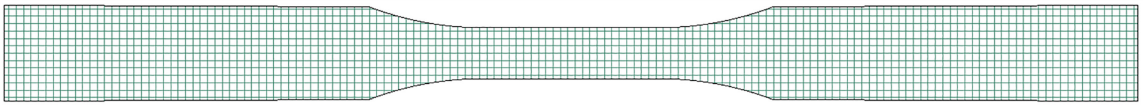

FIG. 7: The 3D virtual S200H specimen with $[0/90]_{2s}$ and 8HSW used in model calibration

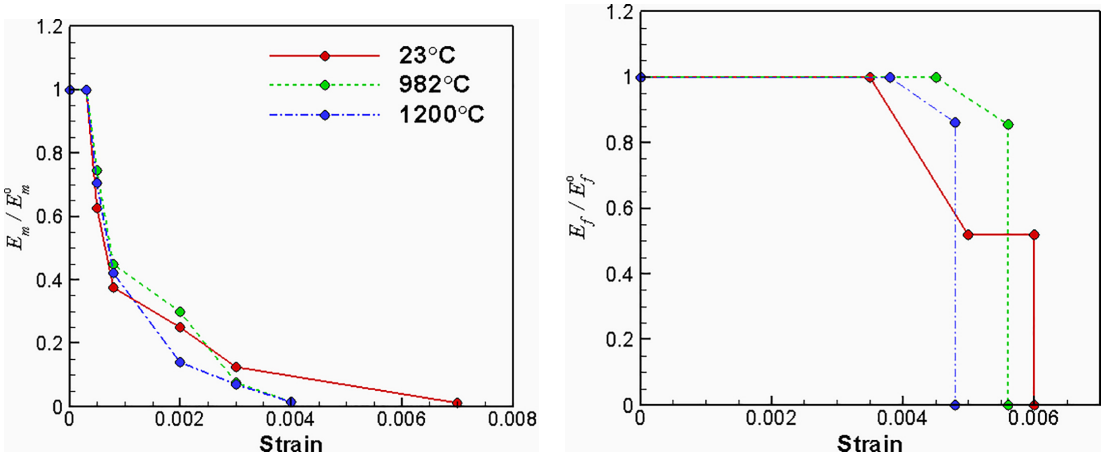

(a) (b)

FIG. 8: Calibrated damage evolution laws for (a) the equivalent matrix E_m and (b) the fiber tows E_f. Here, the superscript "0" of E_m and E_f denotes the undamaged elastic modulus.

TABLE 4: Fiber tow rupture conditions, determined in model calibration for S200H

Temperature (°C)	Fiber tow strain (mm/mm)
23	6.0×10^{-3}
982	5.6×10^{-3}
1200	4.8×10^{-3}

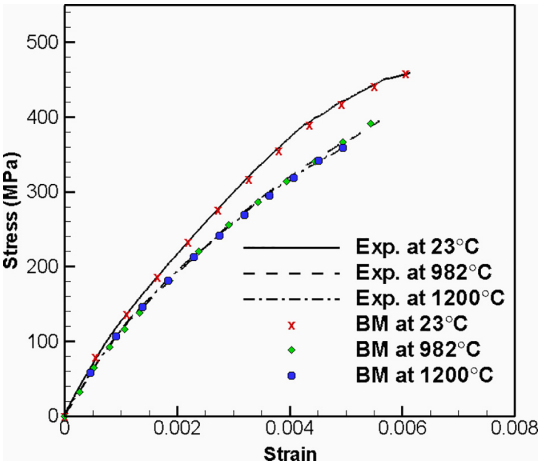

FIG. 9: Experimental measurements (black lines) versus BM predictions (symbols) for the tensile test of S200H

7. BLIND PREDICTIONS

7.1 Blind Predictions for Challenge Problem #1

To conduct blind predictions for a tensile test of GEA SiC/SiC with a unique layup, a 3D virtual specimen was first prepared using the Teledyne composite framework based on the specific features of the test specimen, given in Section 2. The resulting virtual specimen for the tension test of GEA SiC/SiC is visualized in Fig. 10.

Using the BM with the calibrated damage evolution laws for E_m and E_f, FE simulations were carried out to predict the stress–strain responses in GEA SiC/SiC tensile tests at temperatures of 23°C, 816°C, and 1316°C. The simulated stress–strain curves are plotted in Fig. 11. The numerically predicted and experimentally measured tensile properties of GEA SiC/SiC are summarized in Tables 5 and 6, respectively, for comparison purposes. Here, note that the maximum stress point in the simulated stress–strain curve was chosen as the ultimate fracture point. According to the blind prediction results, Young's modulus at each temperature is predicted within about 10% of the validation data, while σ_{PL} (proportional limit stress), σ_{UTS} (ultimate tensile strength) and e_F (strain to failure) are somewhat underpredicted overall. The stress–strain curves seem to be more comparable at elevated temperatures.

The fiber tows of the BM approach, simplified by 1D line elements in FE modeling, characterize only the axial stiffness of the tows. Due to the nature of the 1D fiber tow elements, they undergo translation and rotation (rigid body motion) under the shear deformation of composites, which means shear stress is not taken into account. Due to this shortcoming, the fiber tows with the 30° and 60° orientations on GEA SiC/SiC do not accurately represent the actual mechanical behavior of the composite under tensile loading. After all, the failure of the fiber tows with 0° orientation, which is dominant in the tension test, yields the early failure of GEA SiC/SiC in simulations when compared to validation data.

Finally, Fig. 12 captures the instantaneous local strain ε_{xx} on the equivalent matrix [Fig. 12(a)] and the fiber tows [Fig. 12(b)] of the GEA SiC/SiC specimen at 23°C, just before failure. The antisymmetric strain distribution pattern is observed in the specimen mainly due to the unique unbalanced layup of the composite. Here, the severe damage region coincides with the high strain concentration. Similar behavior is also observed at temperatures of 816°C and 1316°C (but not shown).

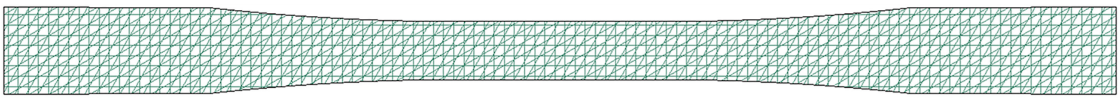

FIG. 10: The 3D virtual GEA SiC/SiC specimen with an unbalanced symmetric layup of $[0/30/60/90]_s$ and a unidirectional weave for a tensile test

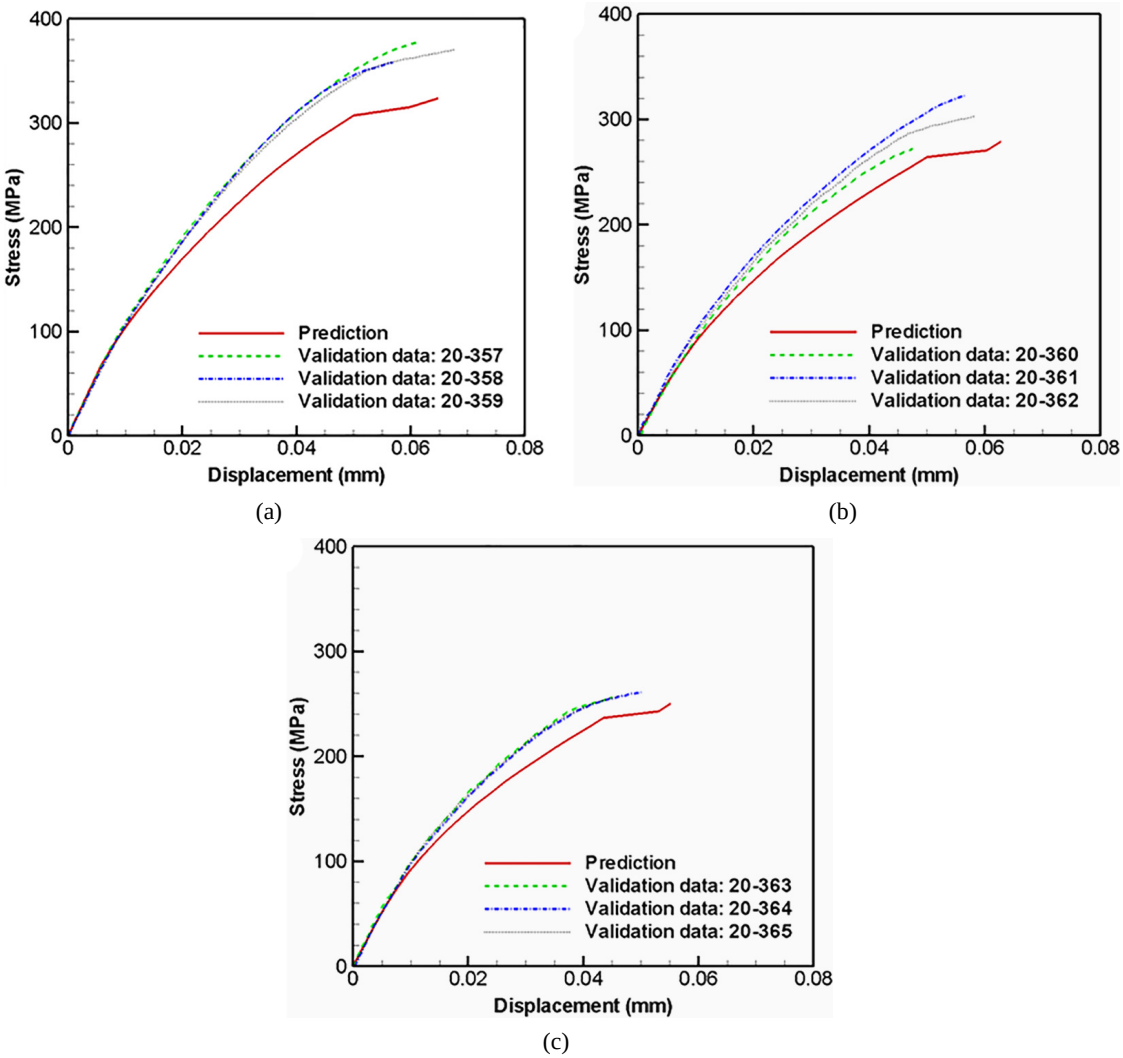

FIG. 11: BM-predicted stress–strain responses for the tensile test of GEA SiC/SiC at three different temperatures of (a) 23°C, (b) 816°C, and (c) 1316°C

TABLE 5: Tensile properties from blind predictions

Temperature (°C)	E (GPa)	σ_{PL} 0.005% (MPa)	σ_{UTS} (MPa)	e_F (%)
23	244.2	172.1	273.7	0.42
816	236.2	156.7	259.7	0.32
1316	216.3	92.5	184.8	0.18

TABLE 6: Tensile properties from validation data (averaged)

Temperature (°C)	E (GPa)	σ_{PL} 0.005% (MPa)	σ_{UTS} (MPa)	e_F (%)
23	249.5	200.7	349.1	1.1
816	236.8	192.5	296.3	0.98
1316	189.4	149.8	198.1	0.86

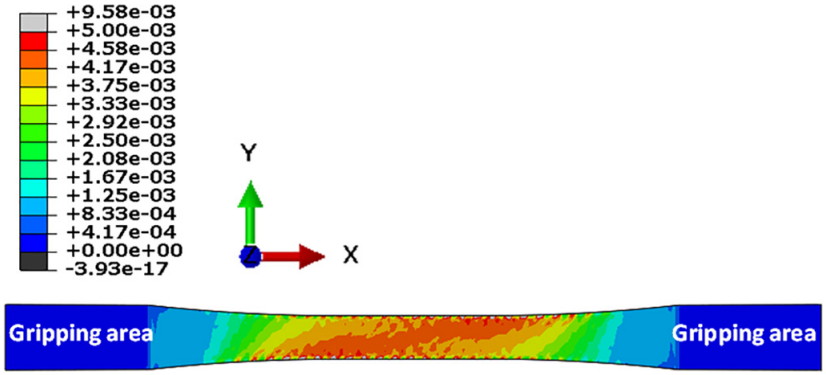

(a)

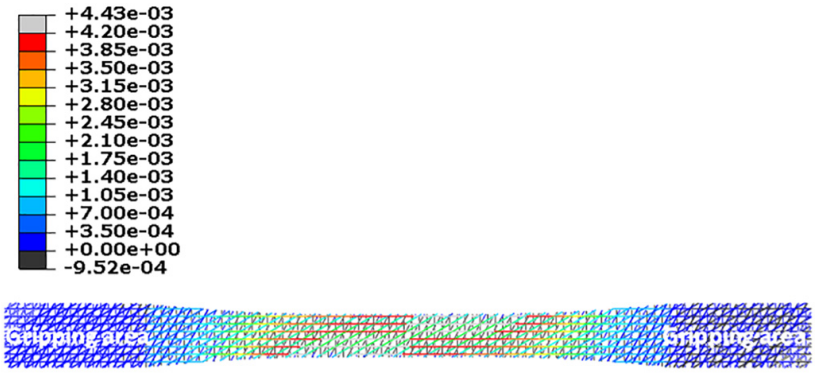

(b)

FIG. 12: The BM-predicted local strain distribution ε_{xx} on the GEA SiC/SiC tensile specimen at 23°C, subjected to axial loading just before failure. (a) equivalent matrix E_m; (b) fiber tows E_f.

7.2 Blind Predictions for Challenge Problem #2

Based on the information described in Section 2 about the tensile test specimen of S200H with two staggered holes, a 3D virtual specimen is generated with the Teledyne composite framework. The virtual S200H specimen for the tensile test is displayed in Fig. 13.

The BM with the calibrated E_m and E_f is used to predict the nonlinear mechanical behavior of the S200H specimen at temperatures of 23°C, 982°C, and 1200°C under axial tensile loading. The resulting stress-displacement curves are plotted in Fig. 14. Here, the net width of 8 mm was assumed in calculation of the tensile stress of this composite. The maximum stress point in the simulated stress–strain curve was considered to be the ultimate fracture point, as in the blind prediction for challenge problem #1.

The numerically predicted and experimentally measured tensile properties of the S200H with two holes are summarized in Tables 7 and 8, respectively, for comparison purposes. According to the results, the predictions of the present damage model have about 10% margin of error and show an overall underprediction compared to the validation data. The stress-displacement curves, as shown in Fig. 14, seem to be more comparable at elevated temperatures.

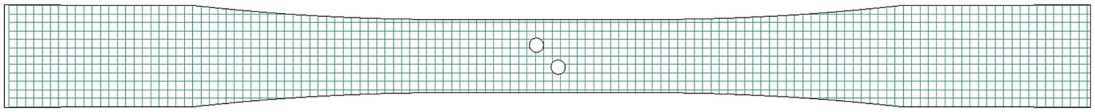

FIG. 13: The 3D virtual S200H specimen with a $[0/90]_{2s}$ layup and an eight-harness satin weave (8HSW) for a tensile test

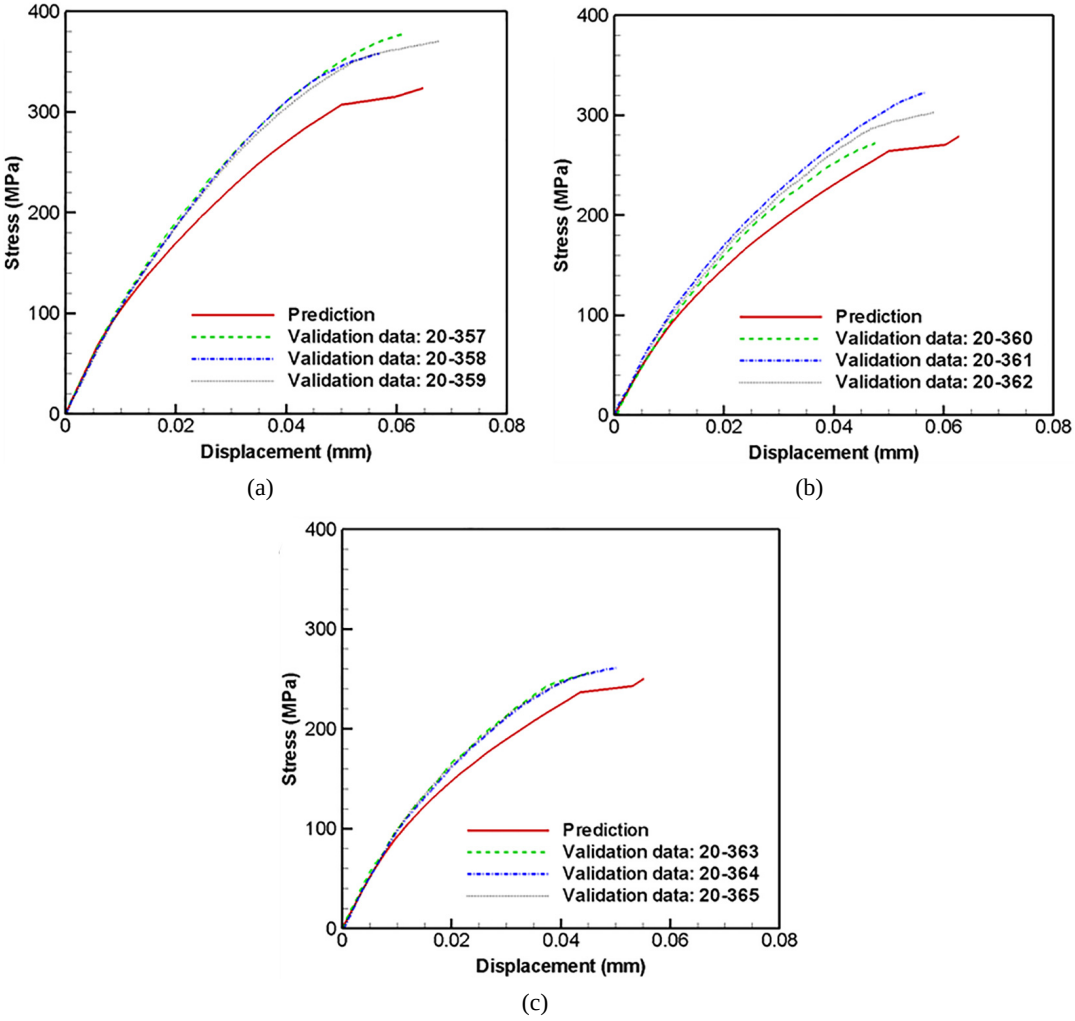

FIG. 14: BM-predicted stress-displacement responses for the tensile test of S200H at three different temperatures of (a) 23°C, (b) 982°C, and (c) 1200°C

TABLE 7: Tensile properties from blind predictions

Temperature (°C)	E (GPa)	σ_{PL} 0.005% (MPa)	σ_{UTS} (MPa)	D_F (mm)
23	141.5	82.14	323.9	0.066
982	120.0	76.05	279.2	0.063
1200	126.4	76.7	250.5	0.055

σ_{PL} is proportional limit stress; σ_{UTS} is ultimate tensile strength; D_F is displacement to failure.

TABLE 8: Tensile properties from validation data (averaged)

Temperature (°C)	E (GPa)	σ_{PL} 0.005% (MPa)	σ_{UTS} (MPa)	D_F (mm)
23	145.0	106.6	368.0	0.063
982	131.8	93.5	298.0	0.055
1200	140.0	83.4	256.7	0.048

As mentioned in Section 7.1, 1D fiber tow elements have a nonshear component due to the nature of a 1D line FE element. Therefore, the 1D fiber tow elements across the loading direction do not accurately represent the actual mechanical behavior of composites in tension. Unlike GEA SiC/SiC with a unique layup of $[0/30/60/90]_s$, S200H consists of only 0° and 90° fiber tow orientations. Also, the 1D fiber tows along the axial loading direction (0°) are dominant in the tension test. Therefore, the material failure prediction of S200H is more comparable to validation data than that of GEA SiC/SiC.

The predicted damage evolution and failure path for the tension test of S200H with two staggered holes at 23°C are illustrated in Fig. 15. The instantaneous local strain ε_{xx} distribution on the equivalent matrix and the fiber tows is captured before [Fig. 15(a)] and after failure [Fig. 15(b)]. Once the high strain/damage concentration occurs at the periphery of the circular holes, perpendicular to the loading direction, the high-damage area initially forms between two open holes and then expands toward the edges of the specimen, as shown in Figs. 15(a) and 15(b). A similar trend was also observed in validation experiments at each temperature (but not shown here).

8. CONCLUSION

A simulation tool plays a key role in the design process of a product, as it can optimize the design for better performance. In that sense, ensuring the accuracy and reliability of a numerical modeling tool for the prediction of damage growth and tolerance in CMCs is undoubtedly important in the development of CMC turbine engine components (Johnson et al., 1998). The strengths and weaknesses of the CDM-based BM approach for progressive damage prediction in CMCs under tension have been identified and discussed in this paper. Newly devised BM-based modeling approaches for creep and fatigue analyses in CMCs are not addressed here and will be discussed in detail in a future publication.

To successfully quantify the strengths and limitations of the CDM-based BM approach, benchmarking exercises have been performed for static analysis for two SiC/SiC CMC systems, namely the GEA SiC/SiC and S200H, using

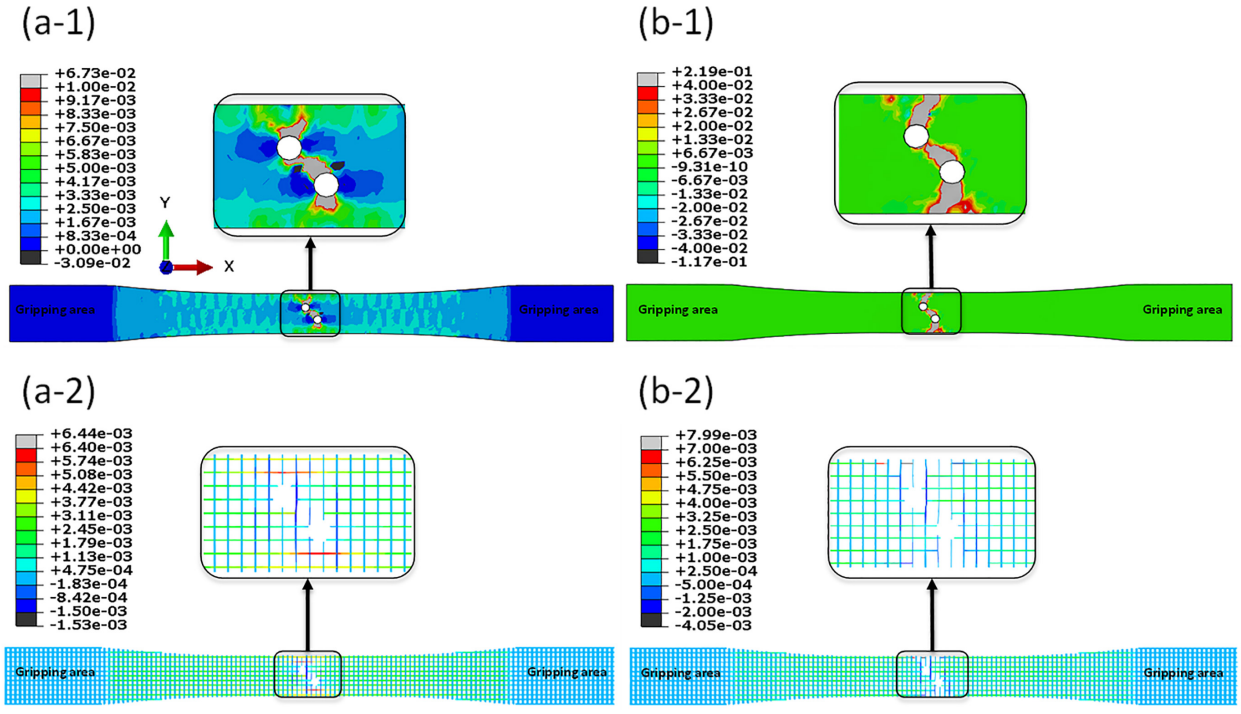

FIG. 15: The BM-predicted local strain distribution ε_{xx} for the S200H tensile test at 23°C under axial loading (a) before and (b) after failure. (a-1) and (b-1): equivalent matrix; (a-2) and (b-2): fiber tows.

the presented modeling approach. The model calibration procedure was established based on the tensile damage mechanisms for CMC materials under tension. The damage evolution laws for the E_m and E_f of the CMCs were determined through the model calibration. The blind predictions were then conducted using the calibrated E_m and E_f. Overall, the blind test results for the challenge problems showed that the current BM approach can capture the failure onset and subsequent damage progression well. In detail, the predicted stiffness and ultimate strength differed from the validation test by $\sim$ 10% on average, while the proportional limit stress (σ_{PL}) and strain/displacement to failure (e_F/D_F) were overall underpredicted in simulations. The fact that 1D fiber tow elements do not incorporate shear stress due to the nature of a 1D truss FE element hinders the accurate prediction of the damage in composites.

In this study, a series of calibration and blind predictions were conducted to benchmark the capability of the TSC damage models (BM-based damage models) for progressive damage prediction in CMCs. A key point in this process is to set up the model calibration process correctly and systematically, considering the feature of the current modeling approaches so that the damage model can accurately represent the actual damage progression of composite materials. In addition, the use of beam elements for fiber tows in the BM framework will help overcome the shortcomings of truss elements that carry only axial stiffness. Unlike truss elements, beam elements can account for shear and bending stiffness of the tows, despite consisting of 1D line elements. However, particular kinematic constraints would be required to impose the compatibility of rotational degrees of freedom between the matrix elements and the embedded tow elements. The development of the embedded element technique for coupling 1D beam elements to solid 3D elements will lead to the improved predictive capabilities of the current BM-based damage modeling approach for CMCs.

ACKNOWLEDGMENT

This work was supported by the ARCTOS Technology Solutions under subcontract 195208-19-08-C1 of the Air Force Research Laboratory Contract FA8650-19-C-5208.

REFERENCES

Cox, B.N., Carter, W.C., and Fleck, N.A., A Binary Model of Textile Composites: I. Formulation, *Acta Metall. Mater.*, vol. **42**, pp. 3463–3479, 1994.

Crété, J.P., Longère, P., and Cadou, J.M., Numerical Modelling of Crack Propagation in Ductile Materials Combining the GTN Model and X-FEM, *Comput. Methods Appl. Mech. Eng.*, vol. **275**, pp. 204–233, 2014.

Department of Defense, *Composite Materials Handbook, Volume 1: Polymer Matrix Composites Guidelines for Characterization of Structural Materials*, Handbook No. MIL-HDBK-17-1F, Washington, DC: U.S. Department of Defense, 2002.

DiCarlo, J.A. and Dutta, S., Continuous Ceramic Fibers for Ceramic Composites, *Handbook on Continuous Fiber Reinforced Ceramic Matrix Composites*, R.L. Lehman, S.K. El-Rahaiby, and J.B. Wachtman, Jr., Eds., West Lafayette, IN: CIAC, Purdue University, pp. 137–183, 1995.

Fang, E., Cui, X., and Lua, J., A Continuum Damage and Discrete Crack-Based Approach for Fatigue Response and Residual Strength Prediction of Notched Laminated Composites, *J. Compos. Mater.*, vol. **51**, pp. 2203–2225, 2017.

Geo, Z., Zhang, L., and Yu, W., A Nonlocal Continuum Damage Model for Brittle Fracture, *Eng. Fract. Mech*., vol. **189**, pp. 481–500, 2018.

Jefferson, G., Przybyla, C., and Zawada, L., Assessment of Damage Progression Models for SiC/SiC Ceramic Matrix Composites, *Int. J. Multiscale Comput. Eng*., 2021. DOI: 10.1615/IntJMultCompEng.2021041807

Johnson, D.W., Evans, A.G., Goettler, R.W., Harmer, M.P., Lipowitz, J.P., Luthra, K., Palmer, P.D., Prewo, K.M., Tressler, R.E., and Wilson, D., *Ceramic Fibers and Coatings: Advanced Materials for the Twenty-First Century*, Publication NMAB-494, Washington, DC: National Academy Press, pp. 12–19, 1998.

McGlockton, M.A., Cox, B.N., and McMeeking, R.M., A Binary Model of Textile Composites: III. High Failure Strain and Work of Fracture in 3D Weaves, *J. Mech. Phys. Solids*, vol. **51**, pp. 1573–1600, 2003.

Murakami, S., Ed., *Continuum Damage Mechanics: A Continuum Mechanics Approach to the Analysis of Damage and Fracture*, Dordrecht: Springer Netherlands, 2012.

Müzel, S.D., Bonhin, E.P., Guimarães, N.M., and Guidi, E.S., Application of the Finite Element Method in the Analysis of Composite Materials: A Review, *Polymers*, vol. **12**, no. 818, 2021.

Pierce, J., Hunt, R., Tandon, G., Jefferson, G., and Zawada, L., Thermo-Mechanical Validation Testing for CMC Progressive Damage Model Benchmarking, *Int. J. Multiscale Comput. Eng*., 2021.

Xu, J., Cox, B.N., McGlockton, M.A., and Carter, W.C., A Binary Model of Textile Composites: II. Elastic Regime, *Acta Metall. Mater.*, vol. **43**, pp. 3511–3524, 1995.

Zivic, F., Busarac, N., Milenkovic, S., and Grujovi, N., General Overview and Applications of Ceramic Matrix Composites (CMCs), *Encycl. Mater.: Compos.*, vol. **2**, pp. 3–19, 2021.

APPENDIX A. TELEDYNE COMPOSITE FRAMEWORK

All virtual specimens used in this numerical study were generated using a custom modeling tool named the Teledyne composite framework. An example for the procedure of generating the virtual specimen with the composite framework is presented in Fig. A1. The composite framework consists of several individual modules performing their own independent tasks. Users can freely connect each module to create their own desired virtual specimens. The specific fabric configuration of the targeted composites is fed into an input of each module, and the virtual specimen is finally cut out from the virtually fabricated composite panel.

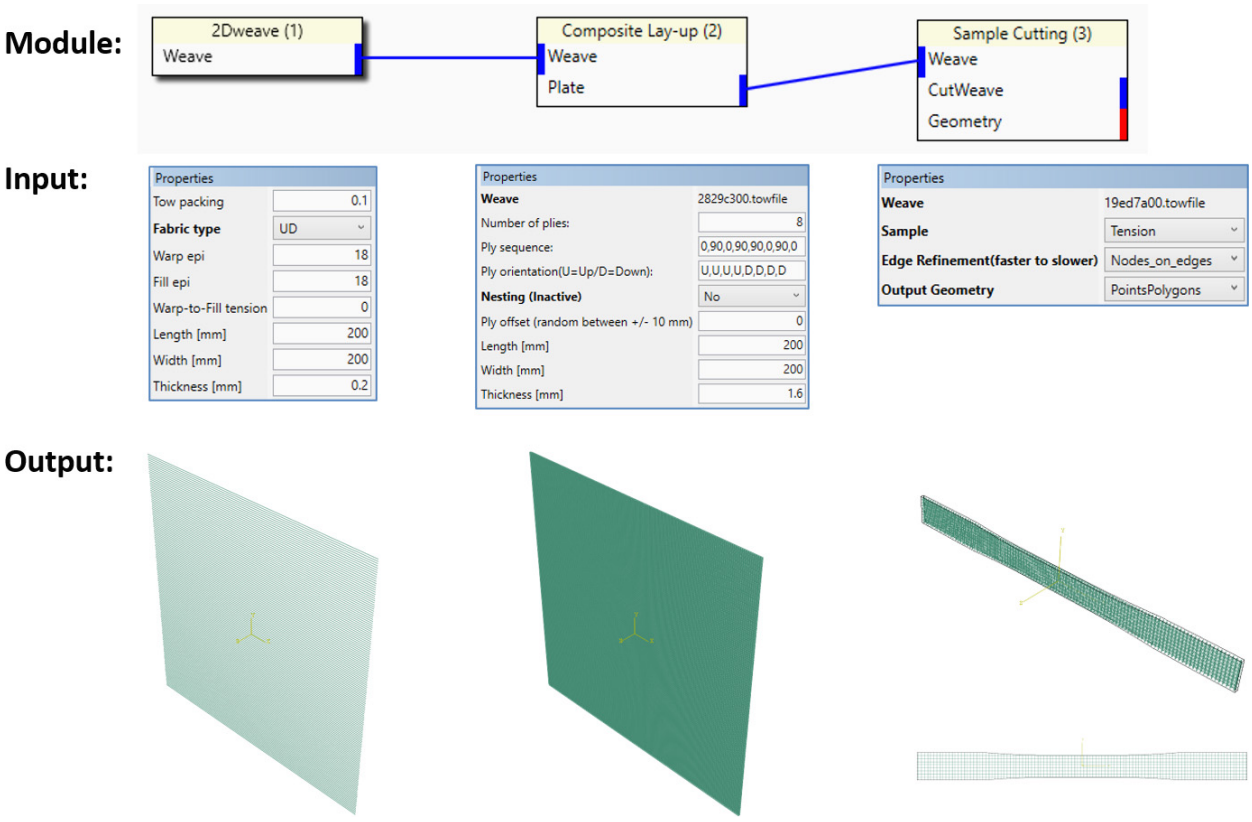

FIG. A1: Example for the generation of a virtual specimen with a layup of $[0/90]_{2s}$ by using Teledyne composite framework